

Integrin-Mediated Signaling Induced by Simian Virus 40 Leads to Transient Uncoupling of Cortical Actin and the Plasma Membrane

Lilli Stergiou^{1*}, Manuel Bauer¹, Waltraud Mair¹, Damaris Bausch-Fluck^{1,3}, Nir Drayman⁴, Bernd Wollscheid^{1,3}, Ariella Oppenheim⁴, Lucas Pelkmans^{1,2*}

1 Institute of Molecular Systems Biology, ETH Zurich, Zurich, Switzerland, **2** Institute of Molecular Life Sciences, University of Zurich, Zurich, Switzerland, **3** National Center of Competence in Research (NCCR) - Neuro Center for Proteomics, UZH/ETH Zurich, Zurich, Switzerland, **4** Department of Hematology, Hebrew University-Hadassah Medical School, Jerusalem, Israel

Abstract

Simian Virus 40 (SV40) is a paradigm pathogen with multivalent binding sites for the sphingolipid GM1, via which it induces its endocytosis for infection. Here we report that SV40 also utilizes cell surface integrins to activate signaling networks required for infection, even in the absence of the previously implicated glycosphingolipids. We identify ILK, PDK1, the RhoGAP GRAF1 and RhoA as core nodes of the signaling network activated upon SV40 engagement of integrins. We show that integrin-mediated signaling through host SV40 engagement induces the de-phosphorylation of Ezrin leading to uncoupling of the plasma membrane and cortical actin. Our results provide functional evidence for a mechanism by which SV40 activates signal transduction in human epithelial cells via integrins in the context of clathrin-independent endocytosis.

Citation: Stergiou L, Bauer M, Mair W, Bausch-Fluck D, Drayman N, et al. (2013) Integrin-Mediated Signaling Induced by Simian Virus 40 Leads to Transient Uncoupling of Cortical Actin and the Plasma Membrane. PLoS ONE 8(2): e55799. doi:10.1371/journal.pone.0055799

Editor: Ludger Johannes, Institut Curie, France

Received: August 14, 2012; **Accepted:** January 2, 2013; **Published:** February 7, 2013

Copyright: © 2013 Stergiou et al. This is an open-access article distributed under the terms of the Creative Commons Attribution License, which permits unrestricted use, distribution, and reproduction in any medium, provided the original author and source are credited.

Funding: This work was supported by the Bonizzi-Theler Foundation (LS), the Swiss National Science Foundation (LP), the National Center of Competence in Research (NCCR) Neural Plasticity and Repair (BW), and the InfectX project within the Swiss Initiative in Systems Biology (BW, LP). The funders had no role in study design, data collection and analysis, decision to publish, or preparation of the manuscript.

Competing Interests: Lilli Stergiou's current employment at Redbiotec AG does not alter the authors' adherence to all the PLOS ONE policies on sharing data and materials.

* E-mail: lucas.pelkmans@imls.uzh.ch

‡ Current address: Redbiotec AG, Zurich-Schlieren, Switzerland

Introduction

Simian Virus 40 (SV40) has served as a paradigm cargo to study caveolae/raft-mediated endocytosis and has revealed many of the features that define this pathway [1–3]. The virus, a DNA non-enveloped member of the polyoma family, binds the glycosphingolipid GM1 as receptor; SV40 virions attach to several GM1 molecules in the outer leaflet of the plasma membrane and are immobilized by the cortical actin cytoskeleton. SV40 uses multiple clathrin-independent endocytic routes, including caveolae, to achieve successful infectious entry [1,3,4]. Uptake of the virus in its host CV1 cells involves activation of a phosphorylation-dependent signaling cascade and local rearrangements of the cortical actin cytoskeleton: filamentous actin is disassembled, followed by recruitment of actin and dynamin II to the cytosolic surface of the caveolae [5]. Moreover, the virus triggers an increase in caveolae dynamics at the cell surface, which promotes exchange between the plasma membrane and cytoplasmic pools of caveolin-1, an effect, which can be mimicked by actin depolymerization [5–7]. Recently, SV40 binding to GM1 was shown to induce membrane curvature that leads to the formation of deep invaginations and tubules, important for successful infection [8]. Furthermore, SV40 infection in cultured HeLa cells was dependent on genes encoding kinases involved in focal adhesion assembly and turnover, and in cell adhesion signaling [9]. A major

undefined aspect of this endocytic uptake route is how it is activated by cargo. There is currently very little knowledge about the molecular identity of the signals that are induced, how these are transduced and regulated, and how this is coupled to downstream effects on the actin cytoskeleton.

To address this we took a two-step approach, using first proteomic technology that would allow for the identification and quantification of cell surface glycoproteins upon virus perturbation, followed by silencing a set of genes, selected and guided by the previous screen, by siRNA in the A431 human epithelial cell line. In this cell line, SV40 infection requires caveolin-1 (Cav1) (see below). Cell biological characterization of the identified genes led us to discover that SV40 requires integrins to efficiently bind to cells. Dependent on both integrins and cholesterol, SV40 induces the phosphorylation of PKB/AKT via the activation of PI3K (phosphatidylinositol 3'-kinase) and PDK1 (3'-phosphoinositide-dependent kinase 1). Via this signaling cascade, SV40 stimulates the Rho GTPase Activating Protein (GAP) GRAF1 to promote the inactivation of RhoA. This, in turn, leads to a loss of phosphorylated Ezrin, resulting in a detachment of the cortical actin cytoskeleton from the plasma membrane, a prerequisite for successful SV40 infection. Because SV40 infection requires Cav1 while the signal transduction induced by SV40 depends on GRAF1, our results reveal a molecular circuitry that combines the

involvement of two proteins associated with different clathrin-independent endocytic activities.

Results

Chemoproteomic Screen Reveals Modulated Plasma Membrane Glycoproteins upon SV40 Entry

To obtain a cell surface subproteome view (“surfaceome”) and to screen for potential changes upon SV40 entry, we used the chemoproteomic Cell Surface Capturing (CSC) technology in combination with quantitative SILAC-based relative quantitative proteomic workflows [10,11]. CSC technology allows for the capturing and subsequent identification of the N-glycosylated surfaceome. Human A431 cells were treated with an infectious SV40 virus stock for 30 min and changes in the surfaceome were monitored in comparison to the uninfected control cells. As a second control, and to detect specific changes during SV40 entry, we performed the same experiment with Vesicular Stomatitis Virus (VSV). These CSC experiments revealed the detectable SV40-modulated A431 surfaceome including, for example, epithelial cell adhesion molecules (EPCAM, CD97), members of the immunoglobulin superfamily (CD58, CD276, EMB, AL-CAM), solute carrier proteins (SLC3A2, SLCO3A1, SLC4A7), and immune response proteins (Interleukin 17A receptor) (Table S1). Among the SV40-modulated proteins we detected and focused on a group of adhesion glycoproteins (Figure 1). Specifically, we observed an increased abundance of six different integrins (ITGA2, ITGA3, ITGA6, ITGB1, ITGB4 and ITGB6) on the cell surface upon 30 min exposure to SV40. These results suggest that either during binding of SV40 to the cell, or during viral entry, SV40 induces a cellular response that leads to a direct, or indirect abundance change of the detected set of glycosylated cell surface adhesion molecules.

RNAi Screen and Epistasis Analysis of Cell Adhesion Components in SV40 Infection

To address whether the observed surfaceome changes have direct functional relevance for SV40 infection, we undertook a candidate-based siRNA screen in A431 cells. For this second screen we generated a gene list based on the following criteria: a) the results of the chemoproteomic screen (first screen) where 11% of the total hits were found to be integrins, b) literature searching for integrin-interacting proteins and cell adhesion molecules, c) extending the STRING network outcome of the molecules above by one or two interactors, and d) including the Rho and Rab GTPase family of signaling proteins, known to regulate SV40 endocytic uptake. A total of 263 genes, transmembrane and structural components, cytoplasmic and signaling molecules of cell adhesion downstream of integrin signaling were compiled (Table S2). These were silenced with 4 individual siRNAs and the effect on SV40 infection was determined with automated microscopy and computerized image analysis. Genes for which at least 2 out of 4 siRNAs significantly changed SV40 infection are listed in a table (Figure 2A).

As expected, this secondary screen revealed the caveolae scaffold protein caveolin-1 (as well as caveolin-3), but also the RhoA GTPase Activating Protein and BAR-domain containing protein ARHGAP26 or GRAF1, known to induce membrane tubulation in clathrin- and caveolin-independent endocytosis [12,13]. Dynamin 1 (DNM1) was also found in this group, consistent with a role for Dynamin in SV40 endocytosis [5]. DNM1, although considered a neuronal dynamin isoform, is expressed in cancer-derived cell lines [14]. Within the set of genes that increased SV40 infection upon silencing we found Ezrin

(EZRIN), a highly expressed protein that establishes a tight coupling between the cytosolic surface of the plasma membrane and the underlying cortical actin cytoskeleton [15,16]. To test genetically whether these proteins might functionally interact, we performed various combinations of double siRNA knockdown. Silencing both Cav1 and GRAF1 did not lead to further inhibition of SV40 infection (Figure 2B), suggesting that these two proteins do not support two parallel pathways of infection. However, we found that loss of GRAF1, but not loss of Cav1, could be efficiently rescued by silencing Ezrin (Figure 2B). This suggests an epistatic relationship in A431 cells where Ezrin lies downstream of GRAF1 in caveolin-dependent SV40 infectious entry.

Integrins are Required for SV40 Binding and are Essential for Infection

To understand how this epistatic relationship might work, we looked for further hints in our screen. We noticed that six integrins were amongst the identified components. Integrins $\alpha 2$ and $\beta 1$ showed a very potent effect, by strongly reducing SV40 infection upon siRNA-mediated silencing (Figure 2A, C). To interfere with integrin function by other means, we used a blocking antibody against $\alpha 2\beta 1$ integrin. Such antibodies have been used to block ligand binding and the functional activity of integrins [17–19]. Pre-exposing cells to this antibody completely blocked SV40 infection (Figure 2C).

When we visualized $\alpha 2\beta 1$ integrins on the cell surface, we observed that in cells that were incubated with SV40, distinct patches of integrins appeared on ruffle-like extensions of the plasma membrane within the first 5 min of virus incubation. This localization persisted for about one hour, after which it disappeared (Figure S1A, and data not shown).

We next performed an assay to determine the binding capacity of SV40 in cells silenced for integrins. $\alpha 2\beta 1$ integrin knockdown compromised SV40 binding to A431 cells, as quantified by western blots against the major capsid protein of SV40, VP1 (Figure 2D). Because literature suggests that integrins might be important to establish levels of GM1 on the cell surface [20,21], and GM1 is currently believed to be the sole attachment factor of SV40 [4,22], we performed the same experiment in GM95 mouse cells, which are deficient in all glycosphingolipids [23].

Remarkably, we observed that SV40 binds quite efficiently to GM95 cells (Figure 2E, Figure S1B), similar to binding in A431 and HeLa cells, although less efficiently than in CV1 cells, which are derived from the natural host of SV40, Green African Monkey. Similar observations were made with recombinant virus-like particles consisting of the outer capsid protein VP1, produced in insect cells [24] (Figure 2F). This indicates that binding of SV40 to GM95 cells is not mediated by a co-purifying contaminant from CV1 cells used to propagate SV40. External loading of GM95 cells with GM1 did however increase the SV40 binding capacity of GM95 cells (Figure 2E), and restored infection in GM95 cells (Figure S1C), in agreement with previous observations [4,22]. When we silenced $\alpha 2$ integrins in GM95 cells, a decrease in SV40 binding was observed (Figure 2G).

To test if SV40 virions and integrins physically interact, we immuno-precipitated $\alpha 2\beta 1$ integrins from A431 cells which were incubated with SV40 for 2 hours on ice. Analysis of the immunocomplexes revealed the presence of SV40 VP1 protein (Figure 2H). Transferrin immunocomplexes, on the other hand, did not contain SV40 VP1 protein (Figure 2H). Together, these results provide experimental cues that integrins could serve as attachment factors of SV40 in the absence of GM1, and that integrins and GM1 could cooperate to increase binding efficiency of SV40 in cells that express both.

A

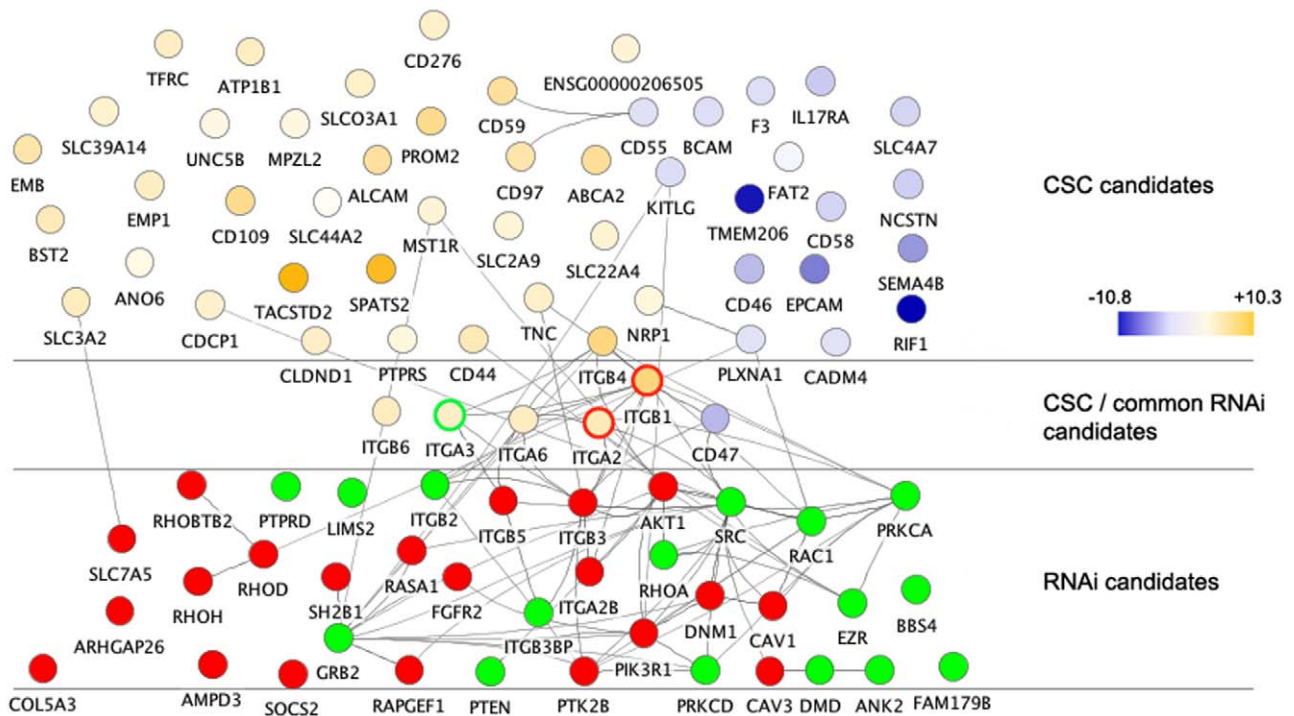


Figure 1. SV40 at its entry triggers the upregulation of a number of integrins on the cell surface. (A) Cell surface N-glycoproteins that are significantly altered in cell surface abundance upon exposure to SV40 are visualized with a network view. The glycoproteins whose abundance was either increased (yellow) or decreased (blue) during exposure to SV40 (and which either did not change during exposure to VSV, or changed in the opposite direction compared to SV40) are depicted as nodes in the network. The different shades represent different degrees of relative abundance (log₂ values). The remaining nodes in the network are the hits from the RNAi screen (see Figure 2A), which either increased (green) or decreased (red) SV40 infection upon siRNA knockdown. For the common hits in the CSC and RNAi screens, the node border represents the RNAi phenotype (ITGA6, ITGB6 and CD47 were CSC-hits but gave no RNAi phenotype when tested). The grey connecting lines between nodes illustrate protein interactions, which were assessed using the STRING database with a combined score of at least 0.9 [45], and were visualized using Cytoscape (www.cytoscape.org) and the Cerebral plugin [46].

doi:10.1371/journal.pone.0055799.g001

SV40 Activates the PI3K-AKT Pathway, which Requires Integrins but not Glycosphingolipids

The list of regulators of SV40 infection also contained members of the PI3K-AKT signaling pathway, one of the major pathways regulating cell survival and growth. Silencing of the serine/threonine protein kinase AKT/PKB, and p85 (PIK3R1), the regulatory subunit 1 of the phosphoinositide 3-kinase (PI3K) reduced SV40 infection (Figure 2A). Silencing of PTEN on the other hand, a phosphoinositide 3-phosphatase and a negative regulator of this pathway, increased SV40 infection (Figure 2A). Additionally, an inhibitor of PDK1 (3'-phosphoinositide-dependent protein kinase 1), which phosphorylates AKT on Thr308 downstream of PI3K, efficiently blocked SV40 infection. An inhibitor of AKT reduced SV40 infection by app. 50% (Figure S2A, B).

This prompted us to look whether SV40 induces the PI3K-AKT signaling pathway in A431 cells. Within 30 min after virus exposure, AKT became phosphorylated at Ser473 in a wortmannin-sensitive manner, indicating that PI3K mediates this event (Figure 3A). This finding is consistent with previous observations [25]. An increase in phosphorylated Tyr458 residues of p85 in the cell periphery demonstrated that PI3K is activated upon exposure to SV40 (Figure S2C). The product of PI3K, PI(3,4,5)P₃, leads to recruitment of AKT/PKB to the cell membrane [26]. Consistent

with this, we observed phospho-AKT (Ser473) associated with the plasma membrane upon SV40 treatment (Figure 3B). This association occurred in a reversible cholesterol-dependent manner (Figure 3B, C), in agreement with observations that this signaling pathway requires cholesterol [27].

Interestingly, when we treated A431 cells with the $\alpha 2\beta 1$ integrin antibody, we were able to induce AKT phosphorylation in a cholesterol-dependent manner even in the absence of SV40 (Figure 3D). Adding SV40 to cells pre-incubated with the $\alpha 2\beta 1$ integrin antibody did not further increase the phosphorylation of AKT (Figure 3D), suggesting that both the virus and the antibody activate AKT via a similar mechanism.

Integrin-mediated phosphorylation of AKT at Ser473 involves integrin-linked kinase (ILK) [28–30], which binds to the cytoplasmic domain of $\beta 1$ integrin. This depends on PI3K [31], presumably to recruit AKT to the membrane in the vicinity of $\beta 1$ integrin-associated ILK. When we silenced either ILK or integrin $\alpha 2$ or $\beta 1$, SV40 was unable to increase the basal levels of Ser473-phosphorylated AKT (Figure 3E, F).

Interestingly, SV40 was also able to induce AKT phosphorylation at Ser473 in GM95 cells, demonstrating that SV40 does not require GM1 or other glycosphingolipids to activate this signaling pathway (Figure 3G). However, in GM95 cells the activation of this signaling pathway could not be blocked by cholesterol

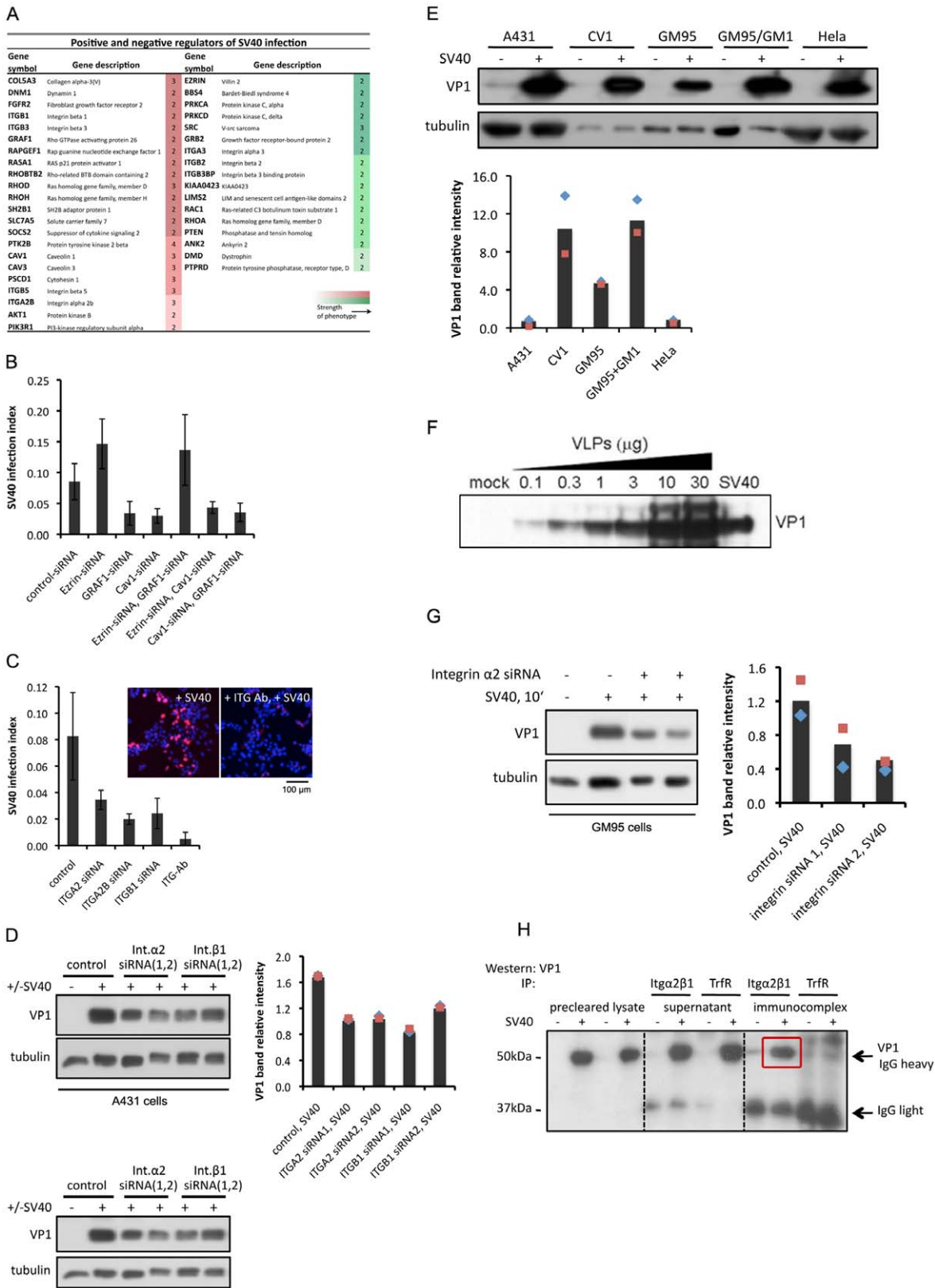


Figure 2. Cell adhesion-signaling components are required for SV40 infection. Integrins, in addition to GM1 lipids, are required for SV40 binding and infection. (A) A targeted siRNA screen reveals several structural and signaling components of cell adhesion to regulate the SV40 infectious route. A set of four siRNAs against 263 genes was applied in A431 human epithelial cells and virus infection was assessed by the presence of nuclear large T-antigen. Low-resolution imaging and image processing with the CellProfiler analysis software were subsequently performed. A Support Vector Machine (SVM)-based classification method [47] was then used to determine percentage of infection upon siRNA treatment. The table

shows the genes that reduced (red shades) or enhanced (green shades) SV40 infection with different strength when knocked down. The values in the boxes represent the number of different siRNAs that gave a similar phenotype. (B) Epistasis analysis between Cav1, GRAF1, and Ezrin. A431 cells were treated with siRNA against each one of these genes or combinations of two. Two or three siRNAs were used per gene. Cells were subsequently treated with SV40 and infection levels were assessed by the presence of nuclear T-antigen. The graph shows values pooled from the individual infection indices. p-values: 1.3×10^{-4} (Ezrin-siRNA, Cav1-siRNA), 0.39 (Ezrin-siRNA, GRAF1-siRNA). (C) Blocking integrin $\alpha 2$ function with an antibody reduces SV40 infection, similar to siRNA-mediated knock down. A431 cells were pre-incubated with 0.02 $\mu\text{g}/\mu\text{L}$ of blocking antibody 20 min prior to infection (p-values 1×10^{-4} – 7×10^{-4}). (D) siRNA against integrins $\alpha 2$ and $\beta 1$ reduces binding of SV40 at the surface of A431 cells. Binding was performed at cold for 2 h and binding capacity was determined by immunoblotting for the presence of the major capsid protein VP1 in cell extracts. Signal intensity was quantified by the ImageJ software and standard deviation corresponds to two independent experiments. (E) SV40 binds onto the surface of various cell lines with different intensity; GM1-deficient cells retain the ability to bind SV40. Quantification of signal intensity from two independent experiments was performed as in (D). (F) SV40-like particles (VLPs) can bind cells that lack its native receptor GM1 in a dose-dependent manner. (G) SV40 can bind cells that lack its native receptor GM1 via integrins. GM95 cells were treated with siRNA against integrin $\alpha 2$ and SV40 binding was determined by the abundance of VP1 protein, as described in (D). (H) Integrins can serve as binding sites for SV40. Integrin $\alpha 2\beta 1$ was immunoprecipitated from A431 cells pretreated for 2 h with SV40 in the cold, and the VP1 protein was detected in the immunocomplex by immunoblotting (red box). Transferrin receptor was used as a negative control. doi:10.1371/journal.pone.0055799.g002

depletion, in contrast to A431 cells (Figure S2D). These results demonstrate that SV40 activates the PI3K-AKT signaling pathway via integrins and ILK, leading to phosphorylation of AKT at Thr308 and Ser473. The activation of this signal does not strictly require glycosphingolipids, and is sensitive to cholesterol depletion only in cells that contain glycosphingolipids.

SV40 Triggers Transient Changes in the Cortical Actin Cytoskeleton by Regulating the Phosphorylation Status of Ezrin

Previous studies have shown that SV40 induces a transient reorganization of the actin cytoskeleton in CV1 cells, an event dependent on plasma membrane cholesterol and protein phosphorylation [5]. Also in A431 cells, SV40 induces a transient reorganization of the actin cytoskeleton (Figure 4A). In these cells, it is visible as a loss of F-actin signal in the cell periphery, the disappearance of F-actin from filopodia-like structures, and the appearance of ruffle-like structures.

The fact that Ezrin, a member of the ERM (ezrin-radixin-moesin) protein family, was amongst the suppressors of SV40 infection (see Figure 2A, Figure S3A, B) suggested that SV40 might achieve this by regulating the activity of Ezrin. ERM proteins serve as linkers between the plasma membrane and the underlying cortical actin cytoskeleton in their active phosphorylated form, and are involved in cell adhesion, membrane ruffling and microvilli formation [15,16].

Using an antibody against Thr567-phosphorylated ERM proteins (phospho-ERM) in A431 cells, we observed a strong signal at the cell periphery and in filopodia. Strikingly, within 5 min after exposure to SV40, the phospho-ERM signal completely disappeared. The signal reappeared after 30 min of continuous exposure to SV40, and was restored after one hour (Figure 4A, B, Figure S3C). Inhibition of type 1 protein phosphatases drastically increased the basal levels of phosphorylated ERM proteins, indicating that ERM proteins are constitutively de-phosphorylated. Inhibition of type 1 protein phosphatases also prevented SV40 from inducing de-phosphorylation of phospho-ERM (Figure S3D). A phosphomimetic mutant of Ezrin (Ezrin-T567D-GFP) remained localized to the cell periphery even in the presence of SV40 (Figure 4C), while a non-phosphorylatable mutant, Ezrin-T567A-GFP, did not localize to the cell periphery even in the absence of SV40 (data not shown). Interestingly, expression of both mutants of Ezrin potently blocked SV40 infection (Figure 4D), suggesting that a full cycle of de-phosphorylation and phosphorylation is required.

These observations indicate that in A431 cells, SV40 activates a signal that results in the transient de-phosphorylation of Ezrin,

leading to a re-localization to the cell interior, followed by phosphorylation and reappearance on the cell surface.

SV40 Induces Ezrin De-phosphorylation via PDK1

We next explored the relationship between SV40-induced activation of the PI3K-AKT pathway and Ezrin de-phosphorylation. When we inhibited PDK1, which transmits the signal from PI3K to AKT, levels of phospho-ERM increased (mean p-ERM intensity: control 27.9%; PDK1 inhibitor 37.0%) (Figure 4E, F). Moreover, treatment of cells with SV40 in the presence of the PDK1 inhibitor failed to trigger de-phosphorylation of phospho-ERM (p-ERM positive cells: SV40-treated 0%; PDK1 inhibitor/SV40-treated 62.0%) (Figure 4E, F). As a note, in addition to Ezrin, Moesin becomes apparent as a higher mobility band on the immunoblot in the presence of the inhibitor (Figure 4F). Similar results were also obtained when cells were exposed to wortmannin to block PI3K function (data not shown). Notably, inhibition of AKT did not prevent SV40 from triggering de-phosphorylation of phospho-ERM (Figure S3E). PDK1, therefore, but not AKT, acts upstream in triggering Ezrin de-phosphorylation. We furthermore observed that the reduction in SV40 infection upon inhibition of PDK1 could not be rescued by additionally silencing Ezrin (Figure 4G), suggesting that PDK1 plays additional roles in SV40 infection apart from enabling the de-phosphorylation of Ezrin.

SV40 Induces Inactivation of RhoA via PDK1 and GRAF1 Leading to Ezrin De-phosphorylation

Besides Ezrin, our screen contained RhoA as a negative regulator of SV40 infection. RhoA has been implicated in regulating the membrane crosslinking function of ERM proteins [15,32]. To test whether SV40 triggers de-phosphorylation of ERM proteins via RhoA, we transiently transfected A431 cells with mutant forms of RhoA. Expression of dominant-active RhoA (RhoA-G14V) led to increased levels of phospho-ERM, and prevented SV40 to induce a reduction of the levels of phospho-ERM (Figure 5A). Expression of dominant-negative RhoA (RhoA-T19N) resulted in loss of phospho-ERM even in the absence of SV40 (Figure 5A). Furthermore, we observed that constitutively active RhoA negatively correlated with SV40 infection, whereas inactive RhoA promoted SV40 infection in the cells it was expressed (Figure 5B). Over-expression of wild-type RhoA displayed a phenotype similar to RhoA-G14V (Figure 5B). These findings indicate that active RhoA keeps ERM in a phosphorylated state, which acts as a barrier to SV40 infection (Figure 4D). Moreover, they are in agreement with the fact that ruffle-like structures are observed in cells treated with SV40 (Figure 4A), presumably due to activation of a small GTPase other than RhoA.

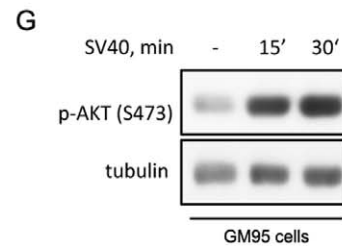
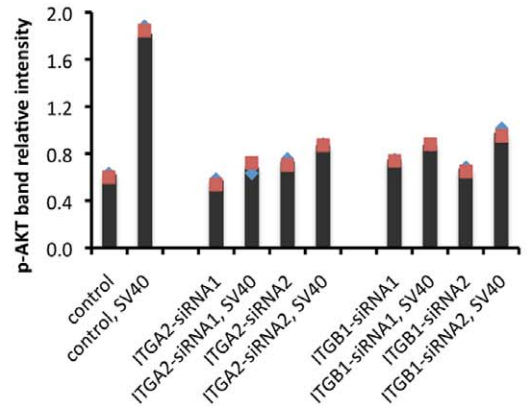
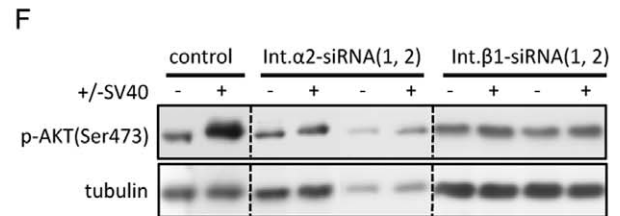
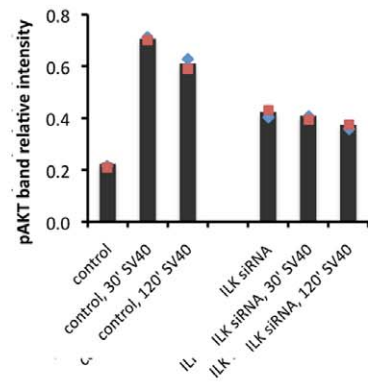
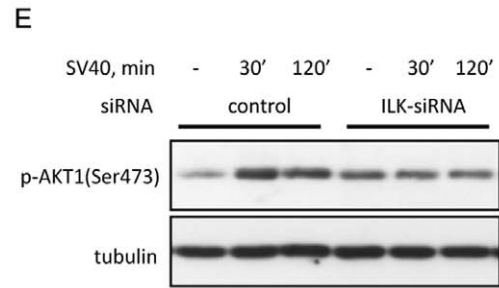
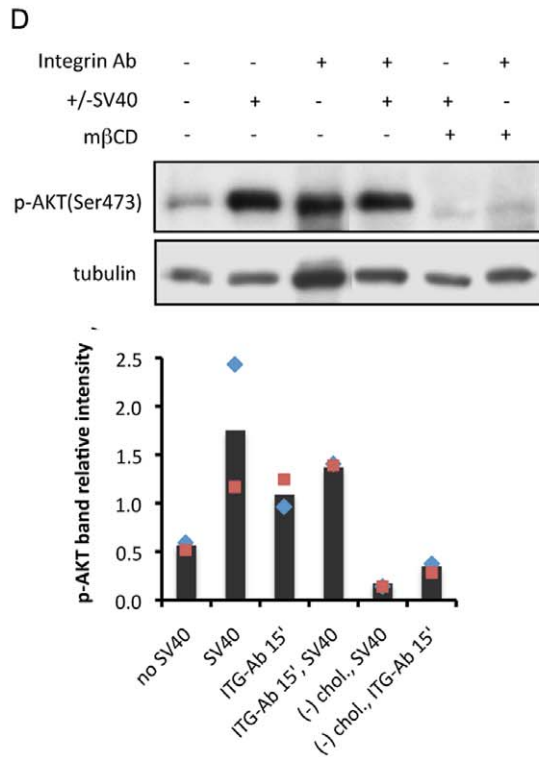
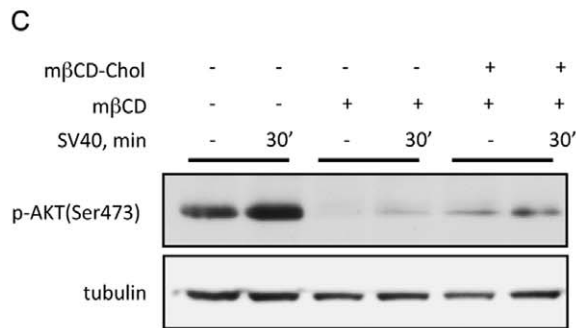
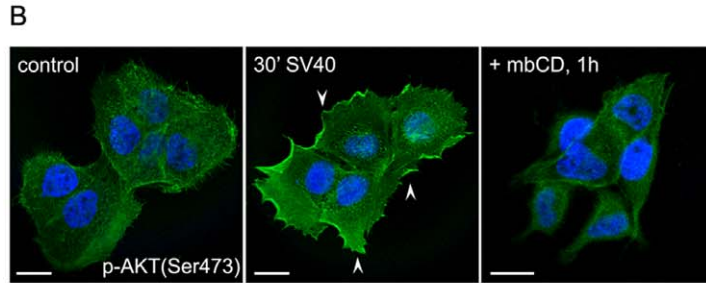
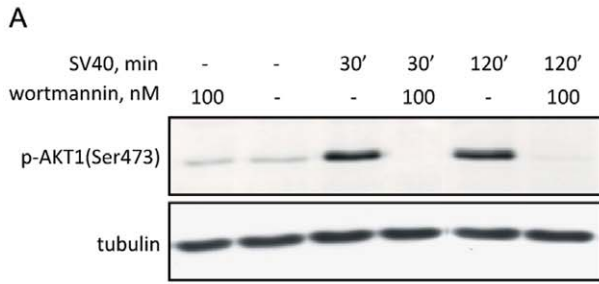


Figure 3. SV40 activates the PI3K/AKT signaling at its entry in A431 and GM95 cells. (A) AKT is activated in a wortmannin-sensitive manner in A431 cells following SV40 treatment. A431 cells were treated with wortmannin for 1 h prior to SV40 treatment. Phosphorylated AKT at Ser473 was tested by immunoblotting. (B, C) Phosphorylated AKT is recruited to the plasma membrane of A431 cells in a cholesterol-dependent manner. p-AKT (Ser473) was detected by immunofluorescence in fixed cells (B) or immunoblotting (C), before or 30 min after SV40 treatment. Cholesterol was extracted from the plasma membrane using methyl- β -cyclodextrin (m β CD) for 45 min. Cholesterol re-administration was succeeded with cholesterol coupled to m β CD for 3 h. Scale bars in (B) represent 15 μ m. (D) Incubating A431 cells with an antibody against integrin α 2 β 1 results in activation of AKT signaling. Incubation was carried out for 15 min before the addition of SV40 for another 10 min. Cholesterol extraction prior to antibody application was performed as described in (B). (E, F) siRNA-mediated knockdown of human Integrin Linked Kinase (ILK) (E) and integrins α 2 and β 1 (F) leads to defective activation of AKT in A431 cells, 10 min following SV40 treatment. (G) AKT is phosphorylated in GM95 cells following SV40 treatment. Quantification of all western blots was done with the ImageJ software; values represent averages of two independent experiments \pm standard deviation.

doi:10.1371/journal.pone.0055799.g003

So far, our observations indicate that PDK1 and inactive RhoA are required to induce de-phosphorylation of ERM proteins by SV40. To connect these observations, we hypothesized that SV40 induces a signal that inactivates RhoA via PDK1 and a GTPase Activating Protein (GAP), leading to a loss of phosphorylated Ezrin, which allows infection to occur. This could explain how the block in SV40 infection upon GRAF1 silencing (Figure S4A, B), which is a GAP of RhoA, is rescued by additionally silencing Ezrin (see the epistasis experiments in Figure 2B). Indeed, we found that in the absence of GRAF1, SV40 cannot induce de-phosphorylation of ERM proteins (p-ERM positive cells: control 91.0%; SV40-treated 0%; GRAF1-siRNA 94.3%; GRAF1-siRNA/SV40-treated 84.6%) (Figure 5C). To test whether PDK1 and GRAF1 are required to inactivate RhoA, we analyzed levels of GTP-bound RhoA in control and SV40-exposed A431 cell lysates. We observed that within 10 min of cell attachment, SV40 induces the partial inactivation of RhoA (Figure 5D) in a transient manner (Figure S4C). SV40-induced reduction of GTP-bound RhoA was abolished by the PDK1 inhibitor and by silencing GRAF1 (Figure 5D). Note that silencing of GRAF1 was more than 2-fold more efficient for siRNA2 (Figure S4B), explaining its more potent effect on RhoA inactivation. Additionally, cells treated with the PDK1 inhibitor or cells silenced for GRAF1, appeared to have less total RhoA (Figure 5D). It is possible that PDK1 and GRAF1 are involved in maintaining total RhoA levels, for instance by preventing its degradation. Furthermore, we observed that over-expressing inactive RhoA (RhoA-T19N) was still able to reduce the number of phospho-ERM positive cells in non-virus-treated cells, even when PDK1 was inhibited or GRAF1 was silenced (Figure 5E, F). This indicates that RhoA acts downstream of PDK1 and GRAF1 in phosphorylating Ezrin. These results indicate that upon SV40 engagement with integrins and activation of the PI3K-AKT pathway, RhoA becomes inactivated downstream of PDK1 and GRAF1, leading to a loss of phosphorylation and dissociation of Ezrin from the plasma membrane.

Discussion

We have here used a chemoproteomic screen in combination with an siRNA screen in order to identify and characterize signaling events induced early upon SV40 entry into host cells. The CSC technology revealed a set of modulated cell surface exposed N-glycoproteins, suggesting that a complex series of events is initiated early during attachment of the virus, which can be detected on the surfaceome level. Specifically, we could show that integrins play a role in signal transduction upon SV40 contact with the host cell, ultimately leading to activation of downstream signaling events. We also observed transient changes in the integrin α 2 β 1 expression pattern at the plasma membrane, presumably reflecting areas of clustered integrins triggered by the virus. Since several viruses use integrins to mediate attachment, cell entry, signaling or endosome escape [33], similar

mechanisms as the ones identified in this study might also apply to other viruses, including members of the polyoma virus family. We currently do not know whether SV40 particles bind directly to integrins, or indirectly via another protein. One possibility is that SV40 binds integrins via extracellular matrix (ECM) proteins such as collagen, since silencing of collagen α V3 impairs SV40 infection (Figure 2A), and mutations in collagen genes from human fibroblasts have been shown to affect organization and clustering of α 2 β 1 integrin receptors [34]. However, collagen may also have a supportive role in signal transduction required for SV40 infectious entry. Importantly, we noticed that the glycosphingolipid GM1 is not strictly required for any of the aforementioned events, and cholesterol is only required for signaling in cells that produce glycosphingolipids. These findings change our view on SV40 entry significantly. They show that SV40 utilizes conventional forms of signal transduction by means of transmembrane proteins. Possibly, a lipid-driven mechanism of membrane invagination that relies on the clustering of lipids [35,36] is required after signal transduction has been initiated and the Ezrin barrier is removed. This would fit our observation that while SV40 can bind and initiate signaling in GM95 cells, it cannot infect these cells without GM1 readministration.

Very early upon SV40 infectious entry, within the first 5 min of membrane attachment and engagement with integrins (and their possible clustering) PI3K is recruited to the membrane. This leads to the downstream phosphorylation of AKT on Ser473 and Thr308, mediated likely by ILK and PDK1, respectively (Figure 6A). Additional signal transduction events involving phospholipase C gamma may also be involved to activate AKT [25]. This membrane-associated signal transduction cascade depends on cholesterol only in cells that produce glycosphingolipids. De-phosphorylation of Ezrin then becomes apparent after 10 min of exposure to SV40, and is achieved downstream of PI3K by PDK1 and GRAF1. PDK1 and GRAF1 are required to inactivate RhoA, inhibiting its activity to maintain phosphorylated levels of Ezrin, most likely via a downstream effector kinase (Figure 6A). The Rho kinase (ROCK) inhibitor Y-27632, however, neither had an effect on levels of phosphorylated Ezrin, nor did it reduce SV40 infection (data not shown), suggesting that ROCK is likely not involved in this step [37]. ERM proteins can, however, be substrates for PKC family members [38,39]. Within 30 min after exposure to SV40, phosphorylated Ezrin reappears, and normal levels are re-established within 1 hour (Figure 6A). Preliminary evidence suggests that the transient nature of this effect is achieved by a feedback loop between Ezrin and PI3K-AKT signaling (not shown and Figure S3F).

Loss and re-establishment of phosphorylated Ezrin may have several consequences: First, the loss leads to an uncoupling of the plasma membrane with the underlying cortical actin meshwork, thus mitigating a barrier for SV40 infectious entry. This is in agreement with the fact that jasplakinolide, which stabilizes the cortical actin cytoskeleton, inhibits SV40 infectious entry [5].

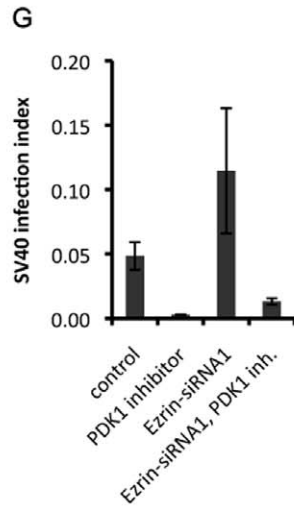
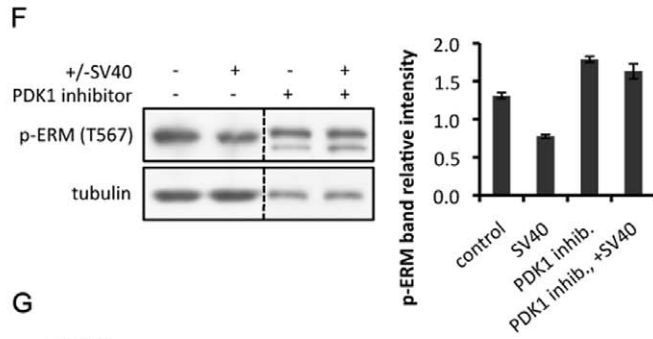
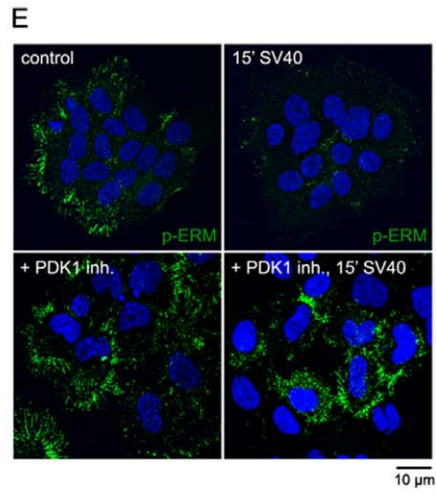
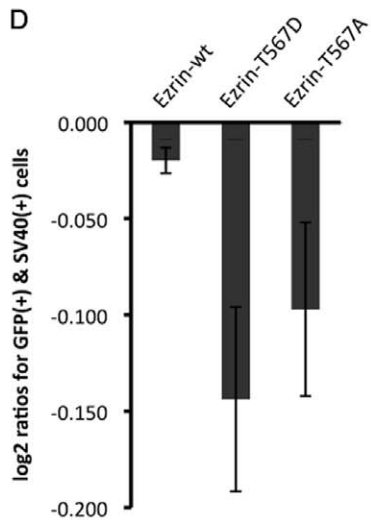
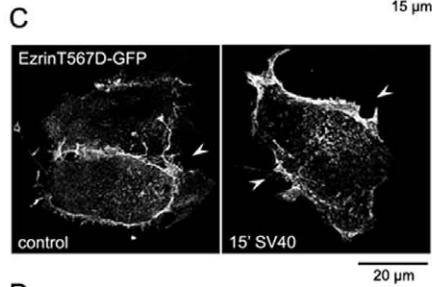
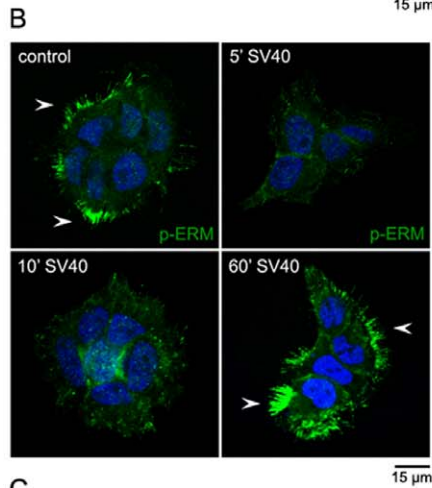
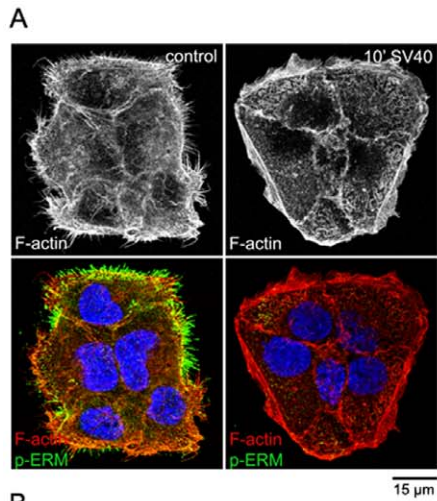


Figure 4. SV40 triggers reversible changes in phospho-Ezrin, dependent on PDK1 function. (A) Cortical actin alterations occur in A431 cells following incubation with SV40 for 10 min, as visualized with phalloidin staining in fixed cells. (B) Phosphorylated ERM proteins become inactive shortly after SV40 treatment. A431 cells were treated with SV40 for the indicated time points, fixed and immunostained with an antibody against phosphorylated T567 of ERM proteins. p-ERM disappears as soon as 5 min after incubation with SV40 and it resumes after 1 h. (C) A phosphomimetic mutant form of Ezrin, T567D, fails to fall off the membrane following SV40 treatment. A431 cells were transfected with EzrinT567D-GFP, treated with SV40 for 15 min, and subsequently fixed and tested for the GFP signal localization. (D) Expression of both a phosphomimetic and an inactive Ezrin mutant form negatively correlates with SV40 infection. Large populations of A431 cells were transfected with EzrinT567D, EzrinT567A or wild-type Ezrin GFP constructs and subjected to SV40. Cells that were both transfected (GFP signal) and infected (T-antigen signal) were scored and compared with the expected number emerging from a random occurrence of the two signals. Negative log₂ ratio values represent an anti-correlation, which demonstrates inhibition of infection by the transfected construct (p-value 6.8×10^{-3} and 0.05 for the T567D and T567A scores, respectively). (E, F) Inhibition of PDK1 function leads to increased levels of p-ERM. The PDK1 inhibitor was applied onto A431 cells for 1.5 h before the addition of SV40 for another 15 min. Levels of p-ERM were assessed using either immunofluorescence in fixed cells (E) or immunoblotting (F). Quantification of two different blots was performed using the ImageJ software. (G) Inhibition of PDK1 function blocks increased levels of infection as caused by Ezrin knockdown. A431 cells were subjected to siRNA against Ezrin or control siRNA, and subsequently treated with the PDK1 inhibitor 1.5 h prior to SV40 infection, or left untreated. Percentage of infection was calculated from a large number of cells. p-values: 1×10^{-4} (PDK1 inhibitor), 5.4×10^{-3} (Ezrin siRNA), 5.8×10^{-4} (Ezrin siRNA, PDK1 inhibitor). doi:10.1371/journal.pone.0055799.g004

Interestingly, we observed that small blebs form on the surface of A431 cells within 10 min of exposure to SV40 (Figure S5A, Movie S1), a well-known consequence of Ezrin de-phosphorylation [40]. Indeed over-expressing a phospho-mimetic mutant of Ezrin severely compromised the formation of blebs in SV40-exposed cells (Figure S5A). Treating SV40-exposed cells with blebbistatin, which inhibits Myosin II and bleb retraction [40], led to the formation of enlarged blebs, and somewhat reduced SV40 infection (Figure S5A, B). Second, we observed that over-expression of phospho-mimetic Ezrin reduces the dynamics of GFP-tagged caveolin-1 (Figure S5C). This suggests that SV40 activates caveolae dynamics by inducing Ezrin de-phosphorylation in cells expressing caveolin-1 [7,41]. Third, we found that energy depletion, known to induce membrane tubulation, leads to a complete loss of phosphorylated Ezrin (Figure S5D, E), suggesting that SV40 activates this signaling pathway to promote membrane tubule formation [8].

Interestingly, although caveolin-1 is essential for SV40 infection in A431 cells, we found it not to be required for the SV40-induced signaling events described here (not shown), in agreement with the fact that inhibition of SV40 infection by silencing caveolin-1 cannot be rescued by additionally silencing Ezrin (see Figure 2B). We neither expect it to be strictly required for virus uptake, since SV40 particles can internalize in caveolin-deficient cells [42], and can be seen in GRAF1-positive intracellular structures in A431 cells (see Figure S4E). An interesting hypothesis that emerges is that bleb formation, induced by SV40, may depend on caveolae, as caveolae can serve as buffers of plasma membrane [43] and their local disassembly may be required for the expansion of plasma membrane during bleb formation. In such a scenario, the signaling pathway activated by SV40 could lead to destabilization of the caveolar coat, which is consistent with our previous findings that SV40 induces the mixing of preassembled caveolar coats [41]. Further work will be required to investigate the role of caveolae in SV40-induced membrane blebbing.

We extensively used phosphorylation of AKT as readout to study the activation of signaling by SV40. However, the actual role of AKT in this network is still elusive. We speculate that it could participate in regulating the endocytic machinery that the virus uses, or is activated by SV40 to maintain pro-survival signals during later stages of infection [25]. The fact that we observe high levels of phosphorylated AKT even after 8 hours of SV40 exposure (not shown) supports the latter. Furthermore, besides Ezrin, we cannot exclude that the other ERM proteins Radixin and Moesin play a role in SV40-induced uncoupling of cortical actin and the plasma membrane. Finally, the interaction between PDK1 and GRAF1, and possibly additional kinases [44] in this signaling pathway require further study. Combining detailed high-

resolution time-lapse imaging with quantitative image analysis of the various molecular players mentioned here, will be necessary to unravel the timing of the here-described signaling pathway and its connection with membrane blebbing and membrane tubulation.

Materials and Methods

Cell Culture

Media and reagents were from GibcoBRL (Paisley, UK). A431 cells were received from ATCC and CV1 cells from ECACC. GM95 cells were obtained from RIKEN BRC. The Cav1-GFP stable cell line was obtained by transfecting the respective construct into A431 cells. All cells were grown in DMEM containing 10% FCS and $1 \times$ Glutamax, and incubated at 37°C under 5% CO₂.

Antibodies and Reagents

Antibodies were from the following sources: rabbit anti-p-ERM: Cell Signaling Technology; mouse anti-p-AKT (S473) and rabbit anti-p-AKT (S473): Upstate, clone 11E6 and Cell Signaling Technology, respectively; anti-p-p85 (Y458): Cell Signaling Technology; mouse integrin $\alpha 2\beta 1$: abcam, clone P1E6; rabbit anti-SV40 VP1: abcam, ab53977; mouse anti-transferrin receptor: Zymed/Invitrogen, 13-6800; rabbit anti-beta tubulin: abcam, ab6046; mouse anti-RhoA: Santa Cruz, clone 26C4; Antisera against viral large T-antigen were provided by Dr. G. Brandner (University of Freiburg, Germany). All fluorescently labeled secondary antibodies were purchased from Molecular Probes and HRP-coupled secondary antibodies were from Jackson Immuno Research Laboratories. The PDK1, AKT and Y-27632 inhibitors were purchased from Calbiochem (124011, 124005 and 688000, respectively). Calyculin A (C-3987) and okadaic acid (O-2220) were obtained from LC Laboratories whereas wortmannin (W1628) and cypermethrin (36128) were purchased from Sigma. GM1 monosialganglioside (G7641) and blebbistatin (B0560) were bought from Sigma. All human and mouse siRNAs were obtained from Qiagen.

Cell Surface Capturing (CSC) Technology

A431 cells that were passaged for at least five generation doublings in SILAC-Medium (Lys, Arg) containing 5% FCS and $1 \times$ Glutamax were used for the experiments. A431 cells were incubated with SV40 or VSV in 50% R-Medium (RPMI, 1% BSA, HEPES pH 6.8) 50% Light Medium or 50% R-Medium 50% Heavy Medium (control) for 45 min at 37°C and 5% CO₂. Cells were washed three times with ice cold labelling buffer (PBS, 0.1% FCS, pH 6.5) and all subsequent steps were performed on ice. CSC was performed as previously described [10,11], with the

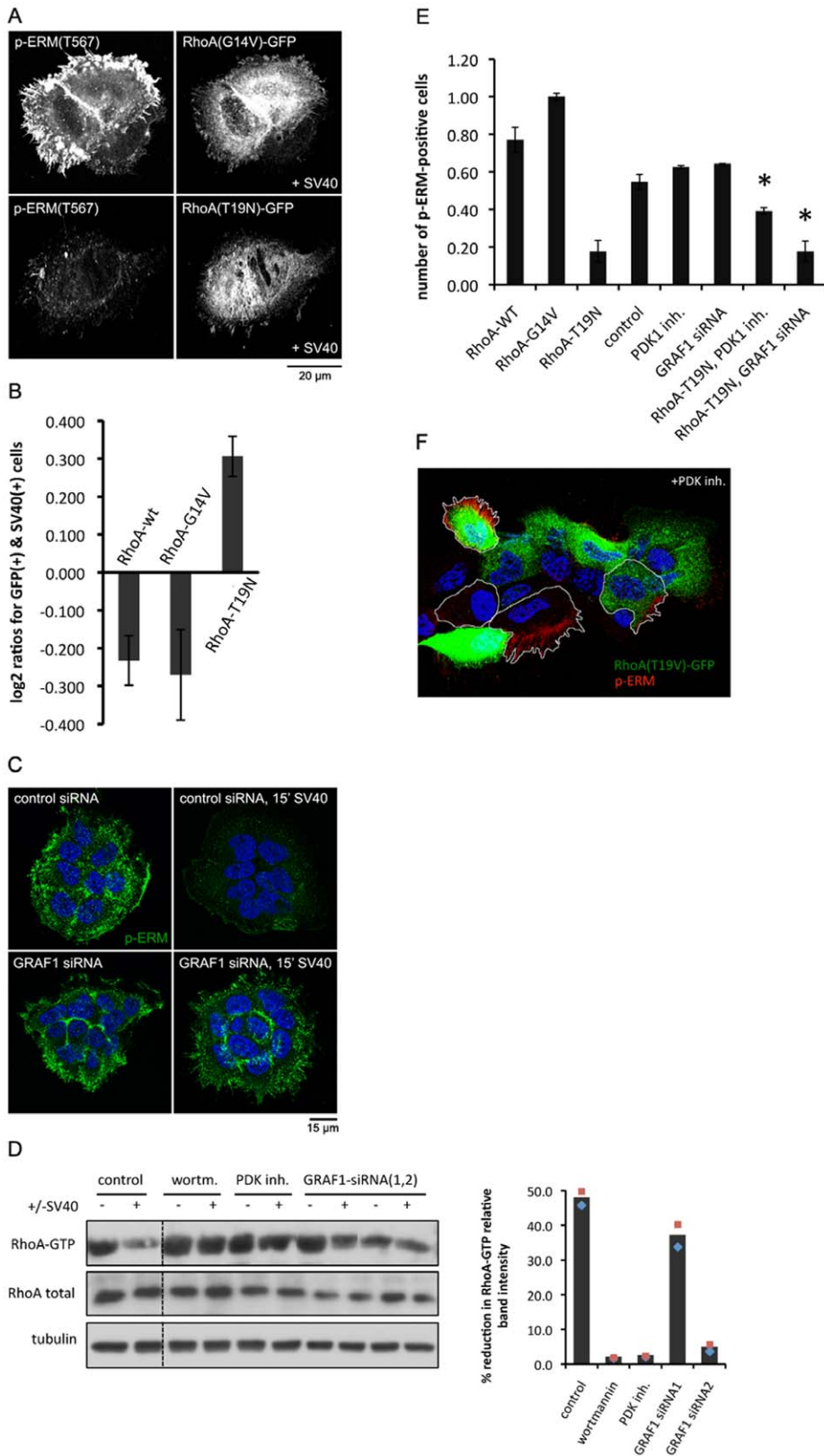


Figure 5. Inhibition of RhoA via GRAF1 promotes Ezrin inactivation and SV40 infection. (A) Constitutively active RhoA leads to increased levels of phosphorylated Ezrin that persist upon SV40 treatment. Inactive RhoA abrogates basal levels of p-ERM. A431 cells were transfected with RhoA-G14V-GFP or RhoA-T19N-GFP before SV40 was applied for 15 min and fixed cells were stained with a p-ERM antibody. (B) Expression of an inactive RhoA mutant form positively correlates with SV40 infection. Large populations of A431 cells were transfected with RhoA-G14V, RhoA-T19N and wild-type RhoA GFP constructs and subjected to SV40. Cells that were both transfected (GFP signal) and infected (T-antigen signal) were scored

and compared with the expected number emerging from a random occurrence of the two signals. Positive log₂ ratio values represent a positive correlation, demonstrating a stimulation of infection, whereas negative values denote anti-correlation, demonstrating an inhibition of infection (p-value 4.2×10^{-4}). (C) Inhibition of GRAF1 function leads to increased levels of p-ERM. siRNA was applied onto A431 cells followed by addition of SV40 for 15 min. Levels of p-ERM were assessed using immunofluorescence in fixed cells. (D) RhoA is inactivated 10 min after SV40 treatment. Inhibition of PI3K and PDK1 with wortmannin or the PDK1 inhibitor, respectively, abolished the SV40-induced reduction in RhoA activity. Cells that had undergone the indicated treatment were subjected to RhoA-GTP immunoprecipitation, which was subsequently detected with a RhoA antibody using immunoblotting. The graph shows the quantification of the RhoA-GTP signal in SV40 exposed cells, as expressed in % reduction compared to the non-treated cells, and normalized against total RhoA and tubulin (quantification based on two different experiments). (E) PDK1 and GRAF1 act both upstream of RhoA to signal to ERM proteins. A431 cells were subjected to the following conditions before being scored for the presence or absence of p-ERM signal using immunofluorescence: transfection with RhoA-WT-GFP, RhoA-G14V-GFP or RhoA-T19N-GFP constructs, incubation with the PDK1 inhibitor for 1.5 h, siRNA treatment against GRAF1, or a combination of RhoA-T19N-GFP expression and the PDK1 inhibitor or GRAF1 siRNA. Acquired confocal images were processed with ImageJ to quantify the number of p-ERM-expressing cells. Inhibition of PDK1 function or silencing of GRAF1 led to partial or no restoration of the fraction of p-ERM-positive RhoA-T19N-expressing cells (asterisks), respectively. Values shown are the average of 2–4 independent experiments \pm standard deviation. (F) Representative image used to extract the values shown in (E). The white line outlines manually segmented cells, whereas green and red depict RhoA-T19N-GFP transfected cells and p-ERM-positive cells, respectively. Dapi-stained nuclei are shown in blue.

doi:10.1371/journal.pone.0055799.g005

following modifications for labelling adherent cells: The cells were oxidized with 1.2 mM NaIO₄ in 3 mL labelling buffer per dish for 15 min with gentle rocking in the dark at 4°C, washed with labelling buffer, and incubated with 24 mM biocytin hydrazide diluted in labelling buffer for 1 h at 4°C, again with gentle rocking. Cells were washed twice, scraped in a total volume of 20 mL hypotonic buffer (10 mM Tris HCl, pH7.5, and 0.5 mM MgCl₂) incubated on ice for 10 min, and homogenized with 40 strokes in a tight-fitting Dounce homogenizer. The postnuclear supernatant was centrifuged in a SW41 rotor (Beckman) at 35,000 rpm for 1 h. Membrane pellets were resuspended and recentrifuged to remove cytoplasmic contamination. Subsequent steps of dissolving in Rapigest, digesting with trypsin, binding to streptavidin beads, washing at high ionic strength, and eluting bound N-glycosylated peptides with protein N-glycosidase F were performed as

previously described [10,11]. Samples were analyzed using a Finnigan LTQ-FT (Thermo Fisher Scientific) mass spectrometer. Peptide identification was performed using the X!Tandem search engine (Version 4.4.0) in combination with PeptideProphet and ProteinProphet software [11]. The relative abundance of the two samples was determined via the XPRESS tool as part of the Trans proteomic pipeline (TPP; version 3.2) [48]. Proteins that were identified by at least one N-glycosylated peptide with a probability cutoff of 0.8 (error rate 0.016), in two or three independent experiments were included in the analysis. The ratios (relative abundance) for all proteins were calculated and used to normalize the results, which are shown as log₂ ratios.

A

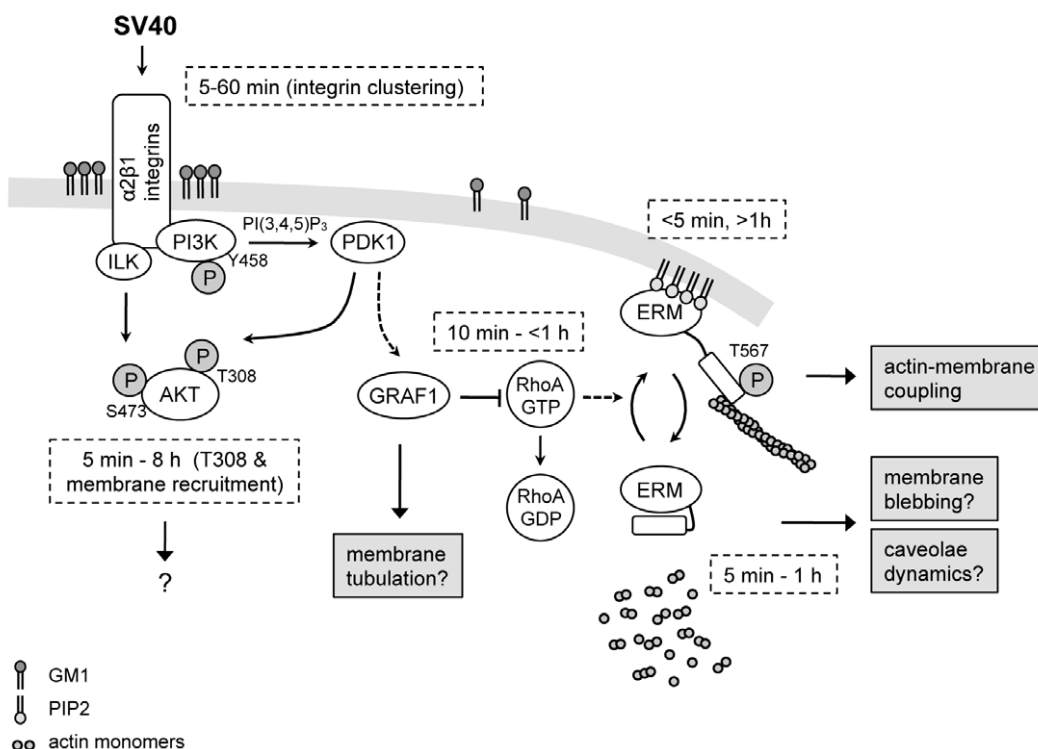


Figure 6. Proposed model of the signaling events upon SV40 infectious entry. (A) The various players participating in the integrin-mediated signaling through host SV40 engagement. The respective time intervals during which these signaling events occur are also depicted. doi:10.1371/journal.pone.0055799.g006

Gene Silencing with siRNA and Candidate-based Screen

All siRNAs were purchased from Qiagen. Cells were reverse transfected with the respective siRNAs in 96-well, 24-well plates or in LabTek chambers. Five, 15 or 7.5 pmol siRNA, respectively, diluted in Opti-MEM and mixed with Lipofectamine 2000 (Invitrogen) were transferred into each well. Cells were seeded on top of the siRNA and incubated for 3 days. For the double siRNA knockdown, 2.5 pmol of each siRNA were used in 96-well plates.

For the candidate-based RNAi screen in A431 cells, 2.5 pmol of four different siRNAs were used to silence each one of 263 genes in 384-well plates. Cells were then infected with SV40 for 22 h, fixed with para-formaldehyde, stained for the presence of large T-antigen, and subsequently imaged with a 10× objective (cell-WoRx, Celloomics). Images were processed with the CellProfiler image analysis software [49]. After nuclei and cell segmentation, based on DAPI and plasma membrane staining, respectively, 133 features including shape, intensity and texture were measured from each object. Those features were used to train a Support Vector Machine (SVM)-based classifier in an iterative manner [47]. Out-of-focus and poorly segmented cells were discarded from the analysis. We used a binary classification approach (infection, no infection) and defined the SV40 infection index as the number of cells with infected nuclei divided by the total number of cells in the well. We defined a lower and an upper threshold according to the infection index of control siRNA-treated cells, and obtained a list with roughly 20 positive and negative regulators of SV40 infection.

Plasmid Construction and Expression of Constructs

The Cav1-GFP construct was described previously [3]. The GFP-GRAF1 construct was kindly provided by Dr. H.T. McMahon (MRC-LMB, UK). The plasmids encoding the PH domain of PLC δ fused to either GFP [50] were kindly offered by Prof. T. Meyer (Stanford University, USA) and Dr. Charras (University College London, UK), respectively. The Ezrin-T567A and Ezrin-T567D sequences were a gift from Prof. T. Ng (King's College London, UK), whereas wild-type Ezrin was PCR-amplified from A431 cells. All sequences were cloned into pcDNA5 vector carrying GFP or mCherry C-terminally, using standard cloning protocol procedures. Cells were transiently transfected with the plasmids using Lipofectamine 2000 (Invitrogen, Carlsbad, CA) according to the manufacturer's instructions and were used for analysis 16–20 h later.

Immunofluorescence and Confocal Microscopy

Cells were grown on 12 mm coverslips until the appropriate assay was performed. They were fixed using either para-formaldehyde 4% at room temperature (RT) or ethylene glycol bis-succinimidylsuccinate (EGS) 10 mM at 37°C, permeabilized with 0.1% Triton X-100 and blocked with 1% BSA. They were subsequently incubated with the primary antibodies for 1.5 h at RT, followed by Alexa Fluor labeled secondary antibodies for 45 min at RT. Coverslips were mounted with Immu-Mount (Thermo Shandon, Pittsburgh, PA). A Leica SP2-FCS confocal microscope equipped with a 63×1.4–0.6 NA, HCX Plan-Apochromat objective and with Argon and HeNe laser was used to visualize fixed samples. For live microscopy experiments, cells were grown in LabTek chamber slides. A Zeiss LSM 510 confocal microscope equipped with a 63×1.4 NA Plan-Apochromat objective and the LSM510 software package (Carl Zeiss Micro-Imaging, Inc.) was used to obtain movies of living cells.

SV40 Infection and Binding Assay

SV40 was obtained from ATCC and propagated in CV-1 cells. Infection assays were carried out in 96-well plates. The virus, diluted in R-medium (RPMI 1640, 10 mM Hepes pH 6.8, 0.2% BSA), was applied onto cells and left for 20 h before fixation. Cells were analyzed for infection by indirect immunofluorescence using antibodies against the SV40 large T-antigen. Scanning was performed with an automated CellWorx microscope (Applied Precision Inc., Washington) with 10×/20× magnification. Per well, 25–36 images were acquired and analyzed using SVM learning. For the experiments with pure and/or fluorescent virus, the preparation that was described in Damm et al. [42] was followed. SV40 binding assays were performed at cold for 2 h with cells grown in 24-well plates. The cells were subsequently harvested for immunoblotting analysis or fixed for immunofluorescence analysis.

Integrin Immunoprecipitation

For the IP experiment cells were incubated with SV40 at cold for 2 h. Cells were then lysed with a buffer containing 50 mM Tris-HCL pH 7.5, 150 mM NaCl, 0.1% SDS, 1% Nonidet P-40, 1% Na deoxycholate and protease inhibitors mix. For 300–500 μ L protein extract, 1–2 μ g of integrin α 2 β 1 antibody (abcam, clone P1E6) were used to immunoprecipitate integrins and the immunocomplex was captured with protein G sepharose beads (GE Healthcare, 17-0618-01). The immunocomplex was then dissociated from the beads with heating and loaded onto an SDS PAGE gel. SV40 was detected on the blot using an antibody against the VP1 protein (abcam, ab53977). Immunoprecipitation of the transferrin receptor was used as a negative control for SV40 binding.

RhoA Activity Assay

Activated RhoA was measured by immunoprecipitating the RhoA-GTP fraction from whole protein cell lysates using Rhotekin RBD agarose beads (Millipore, 14–383). Cells were grown on 24-well plates and were either treated with the PDK1 inhibitor or wortmannin for 1.5 h, or were treated with siRNA against GRAF1 for 3 days. SV40 was added to the cells for the indicated time points. Alternatively, a timecourse of SV40 exposure onto untreated cells was performed. Cells were lysed using Mg²⁺ lysis buffer (25 mM HEPES, pH 7.5, 150 mM NaCl, 1% Igepal CA-630, 10 mM MgCl₂, 1 mM EDTA and 2% glycerol) and incubated with the agarose beads according to the manufacturer's instructions. Levels of RhoA-GTP were quantified with immunoblotting using a RhoA antibody (Santa Cruz, clone 26C4). An aliquot was kept before the Rhotekin RBD binding to assess total levels of RhoA. Tubulin was used as a loading control and to normalize RhoA protein amounts.

Image Analysis

Image analysis of the assays performed in 96-well plates was carried out with the CellProfiler open-source image analysis software [49]. Confocal microscope images as well as Western blots quantifications were analyzed using ImageJ and Photoshop CS3.

Cholesterol Extraction and Cholesterol/GM1 Readministration

Cholesterol was extracted from cells using 10 mM m β CD in SFM for 1 h. For the readministration experiments, cells were incubated in SFM supplemented with 15 μ g/ml cholesterol complexed to 0.37 mM m β CD for 3 h at 37°C. For the SV40 rescuing experiment in GM95 cells, 2.3, 4.6, 9.2 or 13.8 μ M GM1

complexed to fatty acid-free BSA was applied for 12 h onto cells. Incubation with SV40 followed in R-medium devoid of GM1.

Relative Quantification of Transcripts

Cells grown in a monolayer and treated with siRNAs against Ezrin and GRAF1 were washed twice with PBS and harvested by adding 200 μ L of Trizol reagent (Invitrogen) per well in a 24-well plate. Total RNA extraction was performed according to the manufacturer's protocol and reverse transcription was performed using the QuantiTect Reverse Transcription Kit (Qiagen). Quantitative real-time RT-PCR was carried out in an Mx3005P QPCR System (Stratagene) using the following primers: Ezrin forward 5'-CTGCAGGACTATGAGGAGAAGAC-3', Ezrin reverse 5'-AGCCATACGGTCAGCCTCTAG-3', GRAF1 forward 5'-GCTTTGATGTGG AAGCAGTAGAC-3', GRAF1 reverse 5'-TTCACCTCTGGCT GTCTTTGTTCG-3', GAPDH forward 5'-TCAAGGCTGAGAACGGGAAGCTTG-3' and GAPDH reverse 5'-AGCCTTCTCCATGGTGGTGAAGAC-3'. Average fold change was calculated using GAPDH as an internal standard.

FRAP Analysis

For FRAP experiments, A431-Cav1-GFP cells were grown on LabTek chamber slides and transfected with 0.4 μ g of wild-type Ezrin- or Ezrin-T567A/T567D-mCherry using Lipofectamine 2000 (Invitrogen, Carlsbad, CA). SV40 was applied onto cells for 15–45 min prior to analysis. A defined region was bleached at full laser power (100% power, 100% transmission, 20 iterations) using the 488 nm line from a 30 mW Argon/2 laser. Recovery of fluorescence was monitored by scanning the region above at low laser power (50% power, 3% transmission) and by acquiring images every 2.5 sec. Images were processed using Image J (<http://rsb.info.nih.gov/ij/>). Quantification of FRAP experiments was performed by measuring the fluorescence intensity of the whole cell and of the bleached region before, directly after, and during recovery upon bleaching. Relative intensity of fluorescence (RI) was calculated according to the following equation: $RI = (I_{total}[0]/I_{bleached}[0]) \times (I_{bleached}[t]/I_{total}[t])$, where $I_{total}[0]$ is the total intensity of the cell before bleaching, $I_{bleached}[0]$ the total intensity of the bleached region before bleaching, $I_{bleached}[t]$ the intensity of the bleached region at time t , and $I_{total}[t]$ the intensity of the whole cell at time t .

Supporting Information

Figure S1 SV40 induces integrin patch formation at the membrane of A431 cells, and binds the surface of GM1-deficient (GM95) cells. (A) Integrin $\alpha 2\beta 1$ accumulates at distinct patches on ruffle-like extensions in A431 cells 10–20 min after SV40 treatment and disappear again after 1 h. Scale bars represent 15 μ m. (B) SV40 binds the surface of GM95 cells. Cells were incubated with SV40 for 2 h at cold, fixed and subsequently tested for the presence of VP1 protein using immunofluorescence. Arrowheads indicate regions where SV40 particles are bound to cells. (C) Exogenous addition of GM1 rescues the defect in SV40 infection of GM95 cells. Cells were incubated with GM1 for 18 h before SV40 treatment and infection levels were assessed by the presence of nuclear T-antigen (p-value 0.001 for the 9.2 μ M GM1 addition). (TIF)

Figure S2 Inhibitors of PDK1 and AKT reduce SV40 infection. (A) The PDK1 inhibitor efficiently blocks AKT phosphorylation on Thr308, but has no effect on Ser473 phosphorylation. A431 cells were treated for 1.5 h with 10 μ M of

inhibitor before exposed to SV40 for 15 min. p-AKT (Thr308 and Ser473) levels were determined using immunoblotting in two different experiments. Quantification was performed using the ImageJ software. (B) A431 cells were treated with different concentrations of a PDK1 or AKT inhibitor 1.5 h prior to SV40 treatment. Infection levels were assessed by the presence of nuclear T-antigen. p-values: 4.4×10^{-4} (PDK1 inhibitor), 3×10^{-4} (AKT inhibitor) (C) PI3K is activated following SV40 treatment. A431 cells were incubated with SV40 for 30 min. Phosphorylated p85 at Tyr458 was detected in fixed cells using immunofluorescence. (D) AKT activation in GM95 cells is insensitive to cholesterol depletion. Cholesterol was extracted using methyl- β -cyclodextrin (m β CD) for 45 min and cholesterol re-administration was succeeded with cholesterol coupled to m β CD for 3 h. p-AKT was detected by immunoblotting 10 min after SV40 treatment. (TIF)

Figure S3 Ezrin becomes inactivated upon SV40 treatment. (A) Efficiency of siRNA-mediated knockdown of Ezrin in A431 cells. Remaining mRNA levels from siRNA-treated cells were measured with qRT-PCR and results were expressed as fold-downregulation compared to untreated samples. (B) siRNA against Ezrin increases SV40 infection levels. Ezrin was knocked down in A431 cells with two different siRNAs and SV40 infection was assessed by the presence of nuclear large T-antigen (p-value 3×10^{-3} and 4.7×10^{-3} for siRNA1 and siRNA2, respectively). (C) Phosphorylated ERM proteins become inactive shortly after SV40 treatment and phosphorylation resumes after 1 h. A431 cells growing in 96-well plates were treated with SV40 for 5, 10, 15, 20, 30, 60 and 120 min, fixed and immunostained with an antibody against phosphorylated T567 of ERM proteins. Low-resolution imaging of 400–500 cells and image processing with the CellProfiler analysis software were subsequently performed, and the signal intensity on the plasma membrane was calculated. (D) Activation of a phosphatase leads to Ezrin de-phosphorylation. A431 cells were treated with 2.5 μ M okadaic acid, 0.5 μ M calyculin A or 0.5 μ M cypermethrin for 30 min before SV40 incubation for another 10 min. Levels of p-ERM were determined using immunoblotting. (E) The AKT inhibitor has no effect on Ezrin de-phosphorylation. AKT activity was blocked in A431 cells for 1.5 h before treatment with SV40 for 15 min. p-AKT and p-ERM levels were determined using immunoblotting in two different experiments. Quantification was performed using the ImageJ software. (F) Depletion of Ezrin results in loss of phospho-AKT. Ezrin was knocked down in A431 cells with two different siRNAs before cells were exposed to SV40 for 10 min. p-AKT (Ser473) was detected using immunoblotting. (TIF)

Figure S4 Inactivation of RhoA upon SV40 treatment and GRAF1 localization. (A) siRNA against GRAF1 decreases SV40 infection levels. GRAF1 was knocked down in A431 cells with two different siRNAs and SV40 infection was assessed by the presence of nuclear large T-antigen (p-value 4.9×10^{-3} and 8.7×10^{-4} for siRNA1 and siRNA2, respectively). (B) Efficiency of siRNA-mediated knockdown of GRAF1 in A431 cells. Remaining mRNA levels from siRNA-treated cells were measured with qRT-PCR and results were expressed as fold-downregulation compared to untreated samples. (C) RhoA is transiently inactivated after SV40 treatment. Cells exposed to SV40 for the indicated time points were subjected to RhoA-GTP immunoprecipitation, which was subsequently detected with a RhoA antibody using immunoblotting. The graph shows the quantification of the RhoA-GTP signal normalized against tubulin. Note the differences in the loading control, to which RhoA-GTP intensity is

normalized. (D) GRAF1 can be localized in vesicular or tubular structures in CV1 cells. Cells were transfected with a GFP-GRAF1 construct, fixed and imaged with confocal microscopy for the GFP signal localization. Dapi-stained nuclei are shown in blue. Depicted are two examples of untreated cells visible in a population. Scale bars represent 10 μm . (E) SV40 can partition in GRAF1-positive vesicles. A431 cells were transfected with GFP-GRAF1 and subsequently exposed to fluorescently-labeled SV40 (AF568-SV40) for 1 h at 37°C. Fixed cells were then tested for the localization of the virus within GRAF1-positive structures. The arrowhead points to a tubule that also contains SV40 particles. Scale bars represent 15 μm . (TIF)

Figure S5 Consequences of loss and re-establishment of phosphorylated Ezrin. (A) SV40 induces membrane blebbing dependent on Ezrin inactivation. A431 cells were transfected with the PI(4,5)P₂ membrane marker, PH(PLC δ)-GFP, and further incubated with SV40. Live cell imaging was performed during the first 10 min of virus treatment. Addition of 100 μM blebbistatin for 45 min prior to SV40 treatment captured blebs at their expanded phase, whereas co-expression of EzrinT567D-mCherry prevented formation of blebs. (B) Treatment of A431 cells with 100 μM blebbistatin for 2 h prior to SV40 treatment reduces infection by 50% (p-value 0.003). (C) Phosphomimetic Ezrin (T567D) strongly reduces the dynamics of Cav1-GFP, while the non-phosphorylatable mutant (T567A) shows no effect. A Cav1-GFP-expressing A431 cell line was transfected with EzrinT567D-mCherry or EzrinT567A-mCherry and FRAP analysis was used to monitor exchange between cell surface and intracellular pools of caveolae. Expression of phosphomimetic Ezrin greatly reduces Cav1-GFP dynamics. (D) A431 cells were energy-depleted for 30 min using NaN₃ [8], fixed and assessed for p-ERM (T567) signal using immunofluorescence. (E) Protein extracts of A431 cells

following energy depletion were subjected to immunoblotting against p-AKT (Ser473) and p-ERM (T567). Energy depletion leads to complete loss of p-ERM, and loss of p(Ser473)AKT. (TIF)

Table S1 Cell surface proteins regulated by SV40 and VSV. Cell surface glycoproteins regulated by 30 min of SV40 or VSV treatment, as determined by quantitative glyco-capture cell surface proteomics (see Figure 1 for more information). (PDF)

Table S2 Genes tested in the RNAi screen. The genes listed here, a total of 263, were selected to perform a candidate-based siRNA screen upon SV40 infection in A431 cells (XLSX)

Movie S1 Bleb formation on the surface of A431 cells upon SV40 exposure. (AVI)

Acknowledgments

We would like to thank F. Wippich, Dr. P. Liberali and Dr. R. Sacher for critical comments on our manuscript, as well as the members of the Pelkmans lab for discussions. We are thankful to Dr. H.T. McMahon for kindly offering us the GFP-GRAF1 construct, and Prof. T. Ng for the Ezrin-T567A and Ezrin-T567D sequences. Last, we want to acknowledge the Light Microscopy Center of ETH for providing us with confocal microscopes.

Author Contributions

Contributed to proteomics analysis: BW. Revised the manuscript: BW. Contributed to VPL experiment: AO. Conceived and designed the experiments: LS MB LP. Performed the experiments: LS MB WM DBF ND. Analyzed the data: LS MB DBF. Contributed reagents/materials/analysis tools: LS MB ND. Wrote the paper: LS LP.

References

- Anderson HA, Chen Y, Norkin LC (1996) Bound simian virus 40 translocates to caveolin-enriched membrane domains, and its entry is inhibited by drugs that selectively disrupt caveolae. *Mol Biol Cell* 7(11): 1825–1834.
- Chen Y, Norkin LC (1999) Extracellular simian virus 40 transmits a signal that promotes virus enclosure within caveolae. *Exp Cell Res* 246(1): 83–90.
- Pelkmans L, Kartenbeck J, Helenius A (2001) Caveolar endocytosis of simian virus 40 reveals a new two-step vesicular-transport pathway to the ER. *Nat Cell Biol* 3(5): 473–483.
- Tsai B, Gilbert JM, Stehle T, Lencer W, Benjamin TL, et al. (2003) Gangliosides are receptors for murine polyoma virus and SV40. *EMBO J* 22(17): 4346–4355.
- Pelkmans L, Püntener D, Helenius A (2002) Local actin polymerization and dynamin recruitment in SV40-induced internalization of caveolae. *Science* 296(5567): 535–539.
- Mundy DI, Machleidt T, Ying Y-s, Anderson RGW, Bloom GS (2002) Dual control of caveolar membrane traffic by microtubules and the actin cytoskeleton. *J Cell Sci* 115: 4327–4339.
- Pelkmans L, Zerial M (2005) Kinase-regulated quantal assemblies and kiss-and-run recycling of caveolae. *Nature* 436(7047): 128–133.
- Ewers H, Römer W, Smith AE, Bacia K, Dmitrieff S, et al. (2010) GM1 structure determines SV40-induced membrane invagination and infection. *Nat Cell Biol* 12(1): 11–18.
- Pelkmans L, Fava E, Grabner H, Hannus M, Habermann B, et al. (2005) Genome-wide analysis of human kinases in clathrin- and caveolae/raft-mediated endocytosis. *Nature* 436(7047): 78–86.
- Wollscheid B, Bausch-Fluck D, Henderson C, O'Brien R, Bibel M, et al. (2009) Mass-spectrometric identification and relative quantification of N-linked cell surface glycoproteins. *Nat Biotechnol* 27(4): 378–386.
- Hofmann A, Gerrits B, Schmidt A, Bock T, Bausch-Fluck D, et al. (2010) Proteomic cell surface phenotyping of differentiating acute myeloid leukemia cells. *Blood* 116(13): e26–34.
- Lundmark R, Doherty GJ, Howes MT, Cortese K, Vallis Y, et al. (2008) The GTPase-activating protein GRAF1 regulates the CLIC/GEEC endocytic pathway. *Curr Biol* 18(22): 1802–1808.
- Hansen CG, Nichols BJ (2009) Molecular mechanisms of clathrin-independent endocytosis. *J Cell Sci* 122(Pt 11): 1713–1721.
- Scherf U, Ross DT, Waltham M, Smith LH, Lee JK, et al. (2000) A gene expression database for the molecular pharmacology of cancer. *Nat Genet* 24(3): 236–244.
- Tsukita S, Yonemura S (1999) Cortical actin organization: lessons from ERM (ezrin/radixin/moesin) proteins. *J Biol Chem* 274(49): 34507–34510.
- Niggli V, Rossy J (2008) Ezrin/radixin/moesin: versatile controllers of signaling molecules and of the cortical cytoskeleton. *Int J Biochem Cell Biol* 40(3): 344–349.
- Weinreb PH, Simon KJ, Rayhorn P, Yang WJ, Leone DR, et al. (2004) Function-blocking integrin alphavbeta6 monoclonal antibodies: distinct ligand-mimetic and nonligand-mimetic classes. *J Biol Chem* 279(17): 17875–17887.
- Chu JJ, Ng ML (2004) Interaction of West Nile virus with alpha v beta 3 integrin mediates virus entry into cells. *J Biol Chem* 279(52): 54533–54541.
- Siebers MC, Walboomers XF, van den Dolder J, Leeuwenburgh SC, Wolke JG, et al. (2008) The behavior of osteoblast-like cells on various substrates with functional blocking of integrin-beta1 and integrin-beta3. *J Mater Sci Mater Med* 19(2): 861–868.
- Sharma DK, Brown JC, Cheng Z, Holicky EL, Marks DL, et al. (2005) The glycosphingolipid, lactosylceramide, regulates beta1-integrin clustering and endocytosis. *Cancer Res* 65(18): 8233–8241.
- Palazzo AF, Eng CH, Schlaepfer DD, Marcantonio EE, Gundersen GG (2004) Localized stabilization of microtubules by integrin- and FAK-facilitated Rho signaling. *Science* 303(5659): 836–839.
- Smith AE, Lilie H, Helenius A (2003) Ganglioside-dependent cell attachment and endocytosis of murine polyomavirus-like particles. *FEBS Lett* 555(2): 199–203.
- Ichikawa S, Nakajo N, Sakiyama H, Hirabayashi Y (1994) A mouse B16 melanoma mutant deficient in glycolipids. *Proc Natl Acad Sci USA* 91: 2703–2707.
- Sandalon Z, Oppenheim A (1997) Self-assembly and protein-protein interactions between the SV40 capsid proteins produced in insect cells. *Virology* 237(2): 414–21.
- Butin-Israeli V, Drayman N, Oppenheim A (2010) Simian virus 40 infection triggers a balanced network that includes apoptotic, survival, and stress pathways. *J Virol* 84(7): 3431–3442.

26. Stokoe D, Stephens LR, Copeland T, Gaffney PR, Reese CB, et al. (1997) Dual role of phosphatidylinositol-3,4,5-trisphosphate in the activation of protein kinase B. *Science* 277(5325): 567–570.
27. Lasserre R, Guo XJ, Conchonaud F, Hamon Y, Hawchar O, et al. (2008) Raft nanodomains contribute to Akt/PKB plasma membrane recruitment and activation. *Nat Chem Biol* 4(9): 538–547.
28. Hammigan GE, Leung-Hagesteijn C, Fitz-Gibbon L, Coppolino MG, Radeva G, et al. (1996) Regulation of cell adhesion and anchorage-dependent growth by a new beta 1-integrin-linked protein kinase. *Nature* 379(6560): 91–96.
29. Wu C, Dedhar S (2001) Integrin-linked kinase (ILK) and its interactors: a new paradigm for the coupling of extracellular matrix to actin cytoskeleton and signaling complexes. *J Cell Biol* 155(4): 505–510.
30. Legate KR, Montañez E, Kudlacek O, Fassler R (2006) ILK, PINCH and parvin: the tIPP of integrin signalling. *Nat Rev Mol Cell Biol* 7(1): 20–31.
31. Persad S, Attwell S, Gray V, Mawji N, Deng JT, et al. (2001) Regulation of protein kinase B/Akt-serine 473 phosphorylation by integrin-linked kinase: critical roles for kinase activity and amino acids arginine 211 and serine 343. *J Biol Chem* 276(29): 27462–27469.
32. Shaw RJ, Henry M, Solomon F, Jacks T (1998) RhoA-dependent phosphorylation and relocalization of ERM proteins into apical membrane/actin protrusions in fibroblasts. *Mol Biol Cell* 9(2): 403–419.
33. Stewart PL, Nemerow GR (2007) Cell integrins: commonly used receptors for diverse viral pathogens. *Trends Microbiol* 15(11): 500–507.
34. Zoppi N, Gardella R, De Paeppe A, Barlati S, Colombi M (2004) Human fibroblasts with mutations in COL5A1 and COL3A1 genes do not organize collagens and fibronectin in the extracellular matrix, down-regulate alpha2beta1 integrin, and recruit alphavbeta3 Instead of alpha5beta1 integrin. *J Biol Chem* 279(18): 18157–68.
35. Pelkmans L (2005) Secrets of caveolae- and lipid raft-mediated endocytosis revealed by mammalian viruses. *Biochim Biophys Acta* 1746(3): 295–304.
36. Cheng ZJ, Singh RD, Marks DL, Pagano RE (2006) Membrane microdomains, caveolae, and caveolar endocytosis of sphingolipids. *Mol Membr Biol* 23(1): 101–110.
37. Matsui T, Maeda M, Doi Y, Yonemura S, Amano M, et al. (1998) Rho-kinase phosphorylates COOH-terminal threonines of ezrin/radixin/moesin (ERM) proteins and regulates their head-to-tail association. *J Cell Biol* 140(3): 647–657.
38. Simons PC, Pietromonaco SF, Reczek D, Bretscher A, Elias L (1998) C-terminal threonine phosphorylation activates ERM proteins to link the cell's cortical lipid bilayer to the cytoskeleton. *Biochem Biophys Res Commun* 253(3): 561–565.
39. Ng T, Parsons M, Hughes WE, Monypenny J, Zicha D, et al. (2001) Ezrin is a downstream effector of trafficking PKC-integrin complexes involved in the control of cell motility. *EMBO J* 20(11): 2723–2741.
40. Charras GT, Hu CK, Coughlin M, Mitchison TJ (2006) Reassembly of contractile actin cortex in cell blebs. *J Cell Biol* 175(3): 477–490.
41. Tagawa A, Mezzacasa A, Hayer A, Longatti A, Pelkmans L, et al. (2005) Assembly and trafficking of caveolar domains in the cell: caveolae as stable, cargo-triggered, vesicular transporters. *J Cell Biol* 170(5): 769–79.
42. Damm EM, Pelkmans L, Kartenbeck J, Mezzacasa A, Kurzchalia T, et al. (2005) Clathrin- and caveolin-1-independent endocytosis: entry of simian virus 40 into cells devoid of caveolae. *J Cell Biol* 168(3): 477–488.
43. Sinha B, Köster D, Ruez R, Gonnord P, Bastiani M, et al. (2011) Cells respond to mechanical stress by rapid disassembly of caveolae. *Cell* 144(3): 402–413.
44. Shibata H, Oishi K, Yamagiwa A, Matsumoto M, Mukai H, et al. (2001) PKNbeta interacts with the SH3 domains of Graf and a novel Graf related protein, Graf2, which are GTPase activating proteins for Rho family. *J Biochem* 130(1): 23–31.
45. Szklarczyk D, Franceschini A, Kuhn M, Simonovic M, Roth A, et al. (2011) The STRING database in 2011: functional interaction networks of proteins, globally integrated and scored. *Nucleic Acids Res* 39(Database issue): D561–8.
46. Barsky A, Gardy JL, Hancock RE, Munzner T (2007) Cerebral: a Cytoscape plugin for layout of and interaction with biological networks using subcellular localization annotation. *Bioinformatics* 23(8): 1040–2.
47. Rämö P, Sacher R, Snijder B, Begemann B, Pelkmans L (2009) CellClassifier: supervised learning of cellular phenotypes. *Bioinformatics* 25(22): 3028–3030.
48. Deutsch EW, Mendoza L, Shteynberg D, Farrah T, Lam H, et al. (2010) A guided tour of the Trans-Proteomic Pipeline. *Proteomics* 10(6): 1150–1159.
49. Carpenter AE, Jones TR, Lamprecht MR, Clarke C, Kang IH, et al. (2006) CellProfiler: image analysis software for identifying and quantifying cell phenotypes. *Genome Biol* 7(10): R100.
50. Stauffer TP, Ahn S, Meyer T (1998) Receptor-induced transient reduction in plasma membrane PtdIns(4,5)P2 concentration monitored in living cells. *Curr Biol* 8: 343–346.